FIELD OPERABLE HYDROGEN MASER DESIGN

Victor S. Reinhardt, Harry E. Peters, Lawrence A. Birnbaum
NASA/Goddard Space Flight Center, Greenbelt, Maryland 20771

INTRODUCTION

The principal elements of a NASA field operable hydrogen maser are shown in Figure 1. This paper will not dwell on the details of NASA hydrogen masers, this has been discussed elsewhere.[1,2,3,4] Instead, this paper will discuss the design principles involved in two important aspects of NASA hydrogen masers: the elongated microwave cavity and storage bulb and the use of automatic flux tuning.

ELONGATED DESIGN

The elongated design has many advantages. Cavity and bulb elongation tends to reduce magnetic inhomogeneity effects, improves operating parameters, and increase the microwave cavity's mechanical stability. The reduction of inhomogeneity effects is caused by the stretching out along the longitudinal direction of both the cavity field lines and the storage bulb. The principal advantages of the elongated design for improved operating parameters comes from the increased bulb volume and the increased filling factor, η'.

An elongated storage bulb has a larger volume than a spherical storage bulb with the same wall collision rate. This increases the efficiency with which hydrogen atoms are focussed into the storage bulb because the larger bulb volume allows the use of a bulb collimator with a larger entrance aperture to achieve the same bulb escape time.

The filling factor, η', is an important parameter in determining maser performance.[5] Figure 2 shows the optimum η' as a function of cavity elongation for various storage bulb shapes. The storage bulb shapes are shown in Figure 3. For a rounded cylindrical bulb in a two to one cavity, optimum η' is 0.511. This represents a 32% improvement over a spherical bulb in a one to one cavity which has an optimum η' of 0.387. Notice also that even for a one to one cavity, the rounded cylindrical bulb yields an optimum η' of 0.461 which is 19% better than that of a spherical bulb.

To aid others in making their own η' calculations, the authors have collected some of the equations and results of their η' calculations in the Appendix to this paper.

The elongated cavity offers another advantage besides improved η': reduced sensitivity to end plate motion. Figure 4 shows the sensitivity of the frequency of a TE_{011} cavity at 1.42 GHz to changes in cavity length. The length sensitivity of a two to one cavity is about 3 MHz/inch, a factor of ten smaller than the 30 MHz/inch sensitivity of a one to one cavity. Reduced end plate sensitivity is important because mechanical instability problems such as creep at joints, differential expansion effects, and ambient pressure sensitivity effect the cavity frequency through end plate motion.

AUTOMATIC FLUX TUNING

Automatic Flux Tuning or autotuning is used to keep the microwave cavity in a hydrogen maser tuned while the maser is operating. When the flux of atoms in a hydrogen maser is changed, the maser's output frequency will change in proportion to the mistuning of the microwave cavity.[5] An autotuner utilizes this change as an error signal in a servo loop to keep the cavity tuned. There are two types of autotuner, a proportional type which utilizes the magnitude of the frequency change, and a sign averager type which only utilizes the sign of the frequency change. The sign averager type is used in the NP masers and has been discussed in a previous paper.[4] Present NASA masers use the proportional type. The present discussion will be limited to this type.

The block diagram of a proportional autotuner is shown in Figure 5. The control register continuously steps the hydrogen maser between high and low flux and measures the change in maser frequency against a reference oscillator. The control register output in a proportional autotuner is:

$$\Delta N = \frac{2(R-1)}{r(R+1)}\, y + \frac{n_3}{r}$$

where R is the tuning factor,[5] y is the average maser fractional frequency offset, r is the resolution of the register, and n_3 is the measurement noise. The control register outputs ΔN every τ_0 seconds. In a well designed system, most of τ_0 is spent measuring the difference in frequency, typically 80% of τ_0, with the rest of the time used to allow the maser to stabilize after the change in flux. This is important because amplitude to phase conversion in the maser receiver can lead to apparent frequency shifts while the maser amplitude is still settling. In a practical system, it is useful to limit the size of ΔN to keep large noise transients from detuning the maser. The measurement noise, n_3, comes from the reference oscillator and the maser itself. Since only differences in frequency are measured, only changes over the time τ_0 will affect n_3.

The output of the control register is summed in a digital integrator, which for times long compared with τ_0, produces an output given by:

$$N = \frac{1}{\tau_0} \int \Delta N \, dt$$

This output controls a tuning register which controls the cavity frequency. The tuning register output changes the average maser frequency by:

$$y_c = -SN$$

Since the maser frequency changes with time, a noise term, n_1, is added to y_c to give the maser output:

$$y = y_c + n_1$$

Putting these equations together, we obtain a loop equation which in differential form is:

$$\frac{d}{dt} y = \frac{d}{dt} n_1 - Gy + \frac{S}{r\tau_0} n_3 \tag{1}$$

where G, the loop gain is:

$$G = \frac{2S(R-1)}{r\tau_0(R+1)} \tag{2}$$

The reciprocal of the loop gain for this first order loop is the loop time constant:

$$T = G^{-1} \tag{3}$$

One can solve these equations for the different noise processes associated with n_1 and n_3 to obtain the rms fractional frequency fluctuations of the maser output $\langle y^2 \rangle^{1/2}$. No matter what noise processes effect the maser and the reference oscillator, n_3 is effectively a white noise process because of the way the control register operates. Also, if data from both high to low and low to high flux is used, reference drift will not enter into n_3. In analyzing n_1 processes, one need only consider long term processes since the loop time constant is usually such that only long term noise processes are affected by the servo loop. The servo loop turns long term non-stationary noise processes into stationary processes, so $\langle y^2 \rangle^{1/2}$ exists for these processes. Table 1 lists $\langle y^2 \rangle^{1/2}$ for n_3 noise, n_1 drift, n_1 random walk of frequency noise, and n_1 flicker of frequency noise.

Noise processes are not fully described by $\langle y^2 \rangle^{1/2}$; from the equation of motion, one must obtain the autocorrelation function or the spectral density from which the Allan variance can be derived. Table 1 also lists the Allan Variance, $\sigma_y(\tau)$, for each process. Notice that the autotuner converts both n_3 noise and n_1 frequency random walk noise into random telegraph noise whose Allan Variance is:

$$\sigma_y^2(\tau) = \langle y^2 \rangle \, h\,(G\tau)$$

where

$$h(\tau) = \frac{2\tau + 4e^{-\tau} - e^{-2\tau} - 3}{\tau^2}$$

Figure 6 shows a plot of $h(\tau)^{\frac{1}{2}}$. Notice that for $\tau \gg 1$:

$$h(\tau) \simeq \frac{2}{3}\,\tau - \frac{1}{2}\,\tau^2$$

which looks like random walk of frequency noise, and for $\tau \gg 1$:

$$h(\tau) \simeq \frac{2}{\tau} - \frac{3}{\tau^2}$$

which looks like random walk of phase noise. Also notice that $h(\tau)$ is quite flat over several orders of magnitude in the intermediate range of τ. This may explain flicker like behavior of some frequency standards due to slow random telegraph modulation of the frequency. Finally, notice that the autotuner converts flicker of frequency noise into flicker of phase noise when $\tau \gg G$.

Table 1

Autotuner Noise Properties

1. n_3 noise:

$$\langle y^2 \rangle^{1/2} = \frac{\sigma_r (R+1)}{2(R-1)} \sqrt{\frac{\tau_0}{2T}}$$

$$\sigma_r^2 = 2(\sigma_{maser}^2 + \sigma_{ref}^2)$$

Table 1 (Continued)

where σ^2_{maser} and σ^2_{ref} are the appropriate two sample Allan Variance for total sample time $2\tau_0$.

$$\sigma^2_y(\tau) = \langle y^2 \rangle h(G\tau)$$

$$h(\tau) = \frac{2\tau + 4e^{-\tau} - e^{-2\tau} - 3}{\tau^2}$$

2. n_1 drift:

$$Y = DT$$

D = free drift rate

3. n_1 frequency random walk:

$$\langle y^2 \rangle^{1/2} = \sigma_w\left(\frac{3T}{2}\right)$$

$$\sigma_w(\tau) = \text{free } \sigma_y(\tau)$$

$$\sigma^2_y(\tau) = \langle y^2 \rangle \quad h(G\tau)$$

$$h(\tau) = \frac{2\tau + 4e^{-\tau} - e^{-2\tau} - 3}{\tau^2}$$

4. n_1 frequency flicker:

$$\langle y^2 \rangle^{1/2} = \frac{\sigma_f}{2}\left[\frac{\ln(1+\omega_c^2)}{\ln 2}\right]^{1/2}$$

σ_f = free $\sigma_y(\tau)$

ω_c = angular cut off frequency of autotuner mixer

for $\tau \ll T$:

$$\sigma^2_y(\tau) = \sigma_f(\tau)$$

for $\tau \gg T$:

$$\sigma^2_y(\tau) = \frac{\sigma_f^2\, T^2}{4\pi(\ln 2)\,\tau^2}\left[\frac{9}{2} - \ln 2 + 3\ln\left(\frac{\pi\tau}{2T}\right)\right]$$

Let us define optimum performance for any n_1 process as minimizing:

$$\langle y^2 \rangle_{n_1} + \langle y^2 \rangle_{n_3}$$

For each n_1 process, these $\langle y^2 \rangle_{opt}^{1/2}$ are listed in Table 2. Using these values, Figure 7 shows the stability of NASA hydrogen masers calculated for various reference oscillators.

Table 2

Optimum Performance

1. n_1 drift:

$$\langle y^2 \rangle_{opt}^{1/2} = \sqrt{\frac{3}{2}} \left(\frac{\sigma_r^2 \, D \, \tau_0 (R+1)^2}{16(R-1)^2} \right)^{1/3}$$

$$T_{opt} = \left(\frac{\sigma_r^2 \, \tau_0 (R+1)^2}{16(R-1)^2 \, D^2} \right)^{1/3}$$

2. n_1 frequency random walk:

$$\langle y^2 \rangle_{opt}^{1/2} = \left(\frac{\sigma_r \, \sigma_w (3\tau_0) \, (R+1)}{2(R-1)} \right)^{1/2}$$

$$T_{opt} = \frac{\sigma_r \, \tau_0}{\sigma_w (3\tau_0)}$$

3. n_1 frequency flicker:

$$\langle y^2 \rangle_{opt}^{1/2} \simeq \frac{\sigma_f}{2} \left[\frac{\ln(1+\omega_c^2)}{\ln 2} \right]^{1/2}$$

$$T_{opt} \geq \frac{3\sigma_r^2 (R+1)^2 \, \tau_0 \ln 2}{4(R-1)^2 \, \sigma_f^2 \ln(1+\omega_c^2)}$$

APPENDIX

FILLING FACTOR FACTS

The filling factor η' is given by:[5]

$$\eta' = \frac{V_b}{V_c} \frac{\langle H_z \rangle^2_{bulb}}{\langle H_r^2 + H_z^2 \rangle_{cavity}}$$

For a TE_{011} cavity of length d and radius a:[6]

$$H_z = J_0\left(S_{01} \frac{r}{a}\right) \sin\left(\frac{\pi z}{d}\right)$$

$$H_r = -\left(\frac{\pi a}{S_{01} d}\right) J_1\left(S_{01} \frac{r}{a}\right) \cos\left(\frac{\pi z}{d}\right)$$

$$S_{01} = 3.8317$$

$$J_1(S_{01}) = 0$$

$$\omega = c\left[\left(\frac{S_{01}}{a}\right)^2 + \left(\frac{\pi}{d}\right)^2\right]^{1/2}$$

$$d = \frac{pc}{\omega}$$

$$a = \frac{pc}{g\omega}$$

$$g = \frac{d}{a}$$

$$p = \sqrt{S_{01}^2 g^2 + \pi^2}$$

At the hyperfine frequency:

$$\frac{c}{\omega} = 3.359142360 \text{ cm}$$

For centered cylindrical bulbs of radius ρ and length ℓ:

$$\eta' = \left(\frac{16}{S_{01}^2\ \pi}\right) \frac{J_1^2\left(S_{01}\ \frac{\rho}{a}\right)\left(\frac{d}{\ell}\right)\sin^2\left(\frac{\pi\ell}{2d}\right)}{\gamma + \delta/g^2}$$

$$\gamma = 0.25481$$

$$\delta = 0.17129$$

At optimum η' for cylindrical bulbs:

$$\frac{\rho}{a} = 0.450$$

$$\frac{\ell}{d} = 0.7423$$

$$J_1^2\left(S_{01}\ \frac{\rho}{a}\right) = 0.33856$$

$$\eta'_{opt} = \frac{0.133675}{\gamma + \delta/g^2}$$

$$\eta'_{opt}(g = \infty) = 0.5246$$

For any shape bulb, if one makes the scale change on both the bulb and the cavity (see Figure 8):

$$z = G\,z'$$

η' will scale as:

$$\eta'(g) = \left(\frac{\gamma + \delta/4}{\gamma + \delta/g^2}\right)\eta'(g = 2)$$

For elliptical bulbs, this is extremely useful since the scale change takes elliptical bulbs into elliptical bulbs. Figure 9 is a contour chart of η' for ellipsoidal bulbs in a g = 2 cavity. The second digit of η' is printed on the chart. The first digit can be inferred from the zeros on the graph which are filled in to emphasize

the changes in the first digit. For example, the optimum ellipsoid bulb in this chart has $\eta' = 0.46$. The horizontal scale is the semi minor axis of the ellipsoid divided by a from 0 on the left to 1 on the right. The vertical scale is the major axis of the ellipse divided by d from 0 on the top to 1 on the bottom. Using the scaling law and this chart, η' can be determined to two digits for any ellipsoidal bulb for any g.

For rounded cylindrical bulbs, optimum η' occurs as follows:

g	η'	ℓ/d	ρ/a
2	0.461	0.85	0.50
3	0.498	0.80	0.50
4	0.511	0.78	0.50

For a g = 2 cavity, Baker[6] has numerically determined the shape of the bulb which optimizes η'. For this bulb, $\eta' = 0.462$.

REFERENCES

1. V. Reinhardt, D. Kaufmann, W. Adams, J. DeLuca, and J. Soucy, "NASA Atomic Standards Program - An Update," Proceedings of the 30th Frequency Control Symposium, USAEC (Atlantic City, 1976).

2. Harry E. Peters, "Characteristics of Advanced Hydrogen Maser Frequency Standards," Proceedings of the Fifth NASA/DOD Precise Time and Time Interval Planning Meeting, NASA Doc. X-814-74-225, pg. 283 (Greenbelt, 1973).

3. Harry E. Peters, "Topics in Atomic Hydrogen Standard Research and Applications," Proceedings of the Frequency Standards and Metrology Seminar (Quebec, 1971).

4. H. E. Peters, T. E. McGunigal, and E. H. Johnson, "Hydrogen Standards Work at Goddard Space Flight Center," Proceedings of the 22nd Frequency Control Symposium, USAEC (Atlantic City, 1968).

5. D. Kleppner, H. C. Berg, S. B. Crampton, N. F. Ramsey, R. F. C. Vessot, H. E. Peters, and J. Vanier, "Hydrogen Maser Principles and Techniques," Phys. Rev. 138, No. 4A, A972 (17 May 1965).

6. W. Davenport and W. Root, "Random Signals and Noise," McGraw-Hill (New York, 1958).

7. D. Gray, ed., AIP Handbook, McGraw-Hill (New York, 1972).

8. R. Vessot, M. Levine, L. Mueller, and M. Baker, "Design of an Atomic Hydrogen Maser System for Satellite Experiments", Proceedings of the 21st Frequency Control Symposium, USAEC (Atlantic City, 1967).

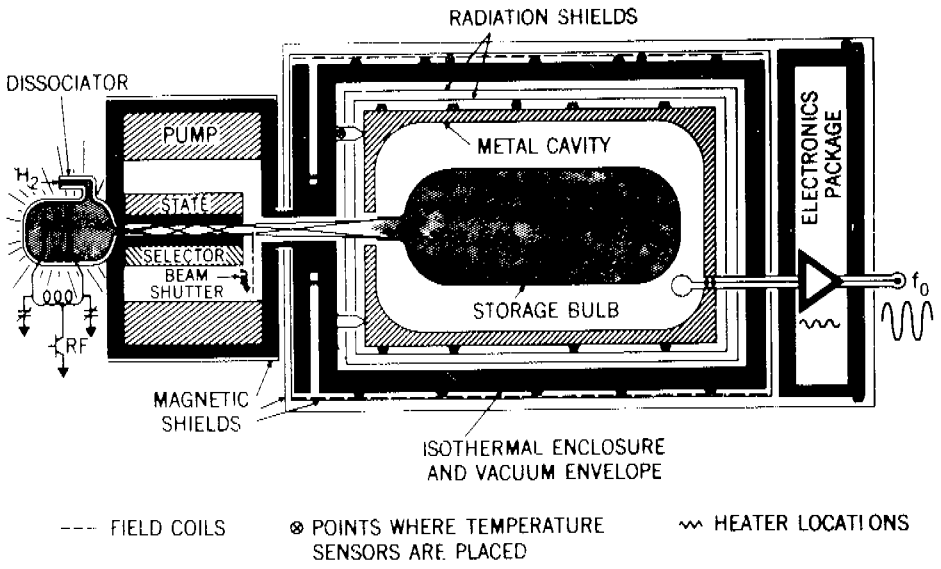

Figure 1. Principal Elements of a NASA Hydrogen Maser

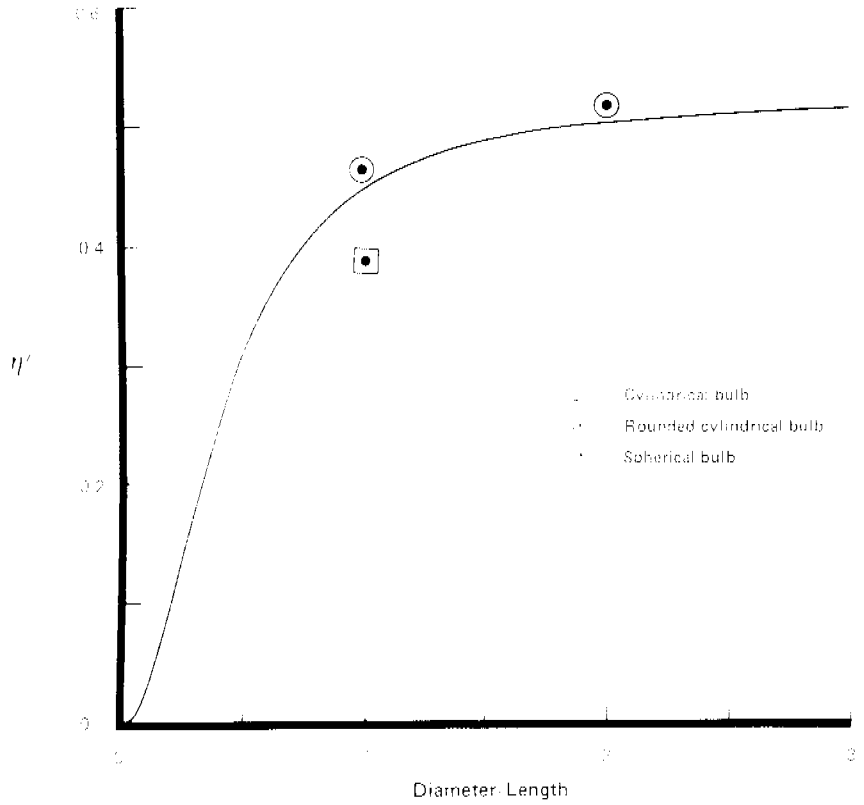

Figure 2. Optimum η' for Various Bulb Types as a Function of Cavity Elongation

Cylindrical

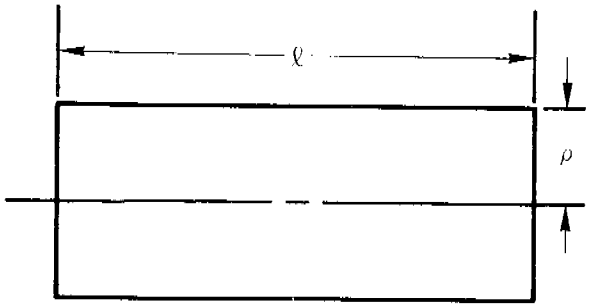

Ellipsoidal

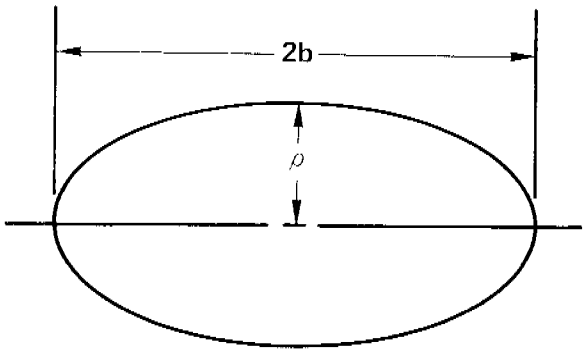

Rounded Cylindrical

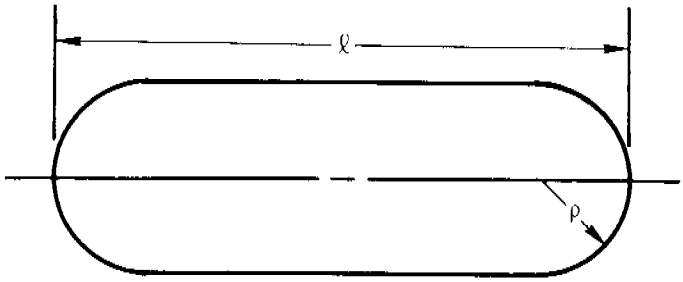

Figure 3. Types of Storage Bulbs

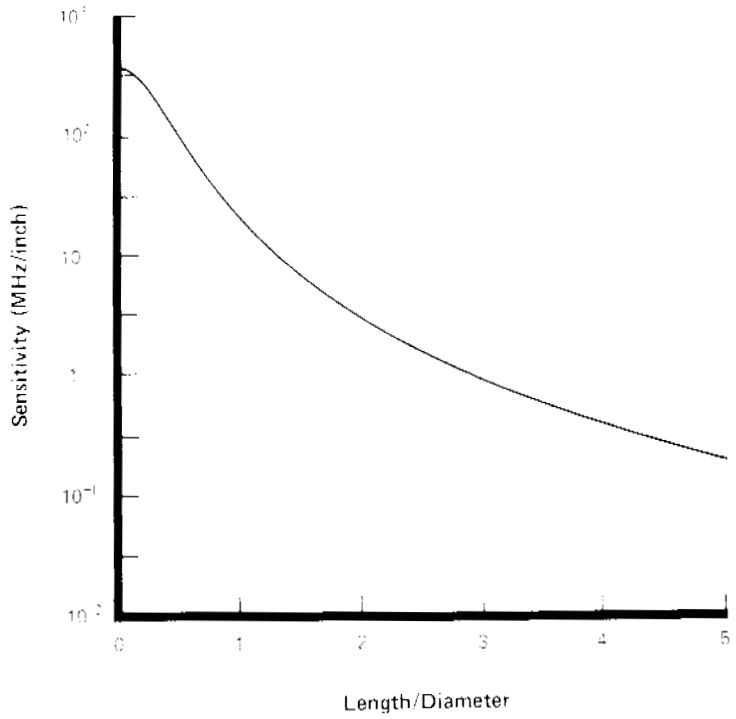

Figure 4. Length Sensitivity Versus Cavity Elongation for a TE_{011} Cavity at 1.42 GHz

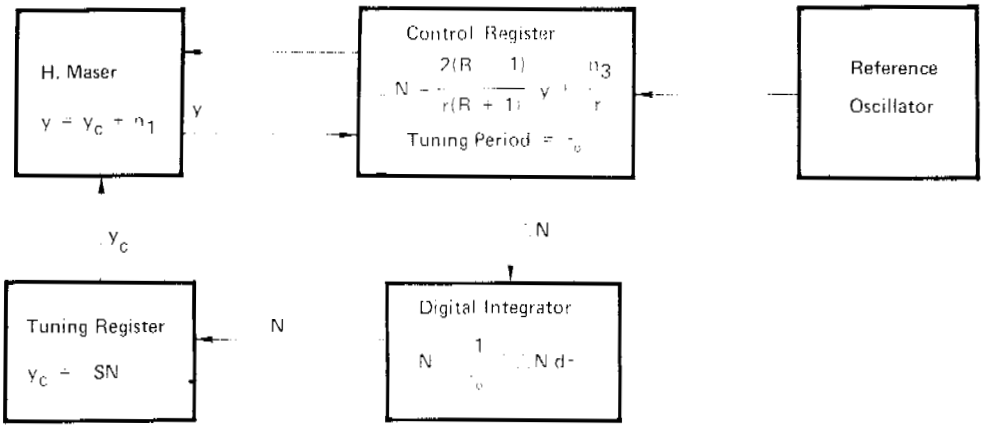

Figure 5. Proportional Autotuner

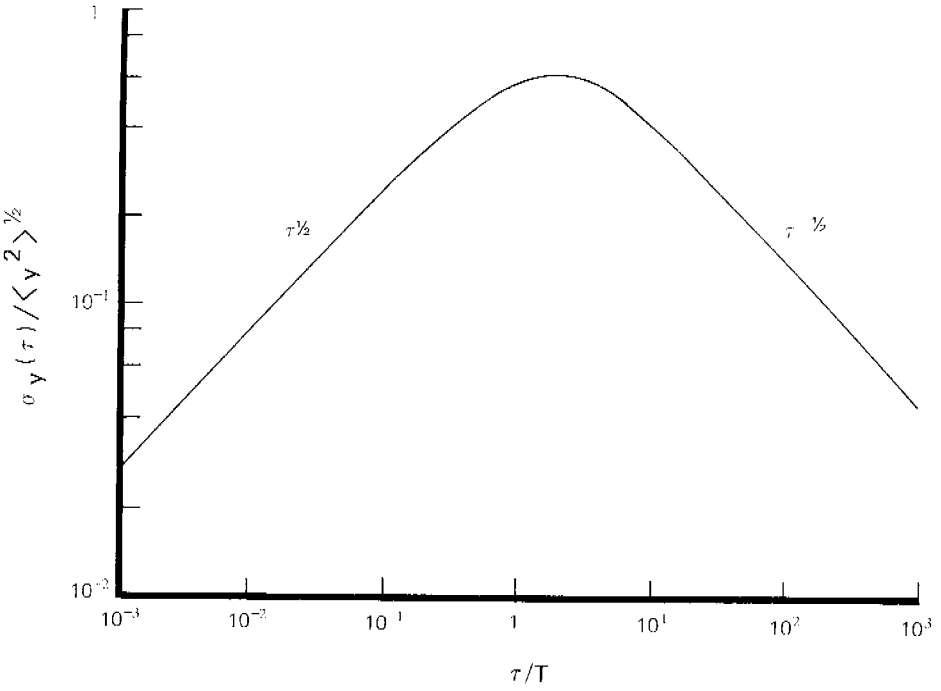

Figure 6. Random Telegraph Allan Variance

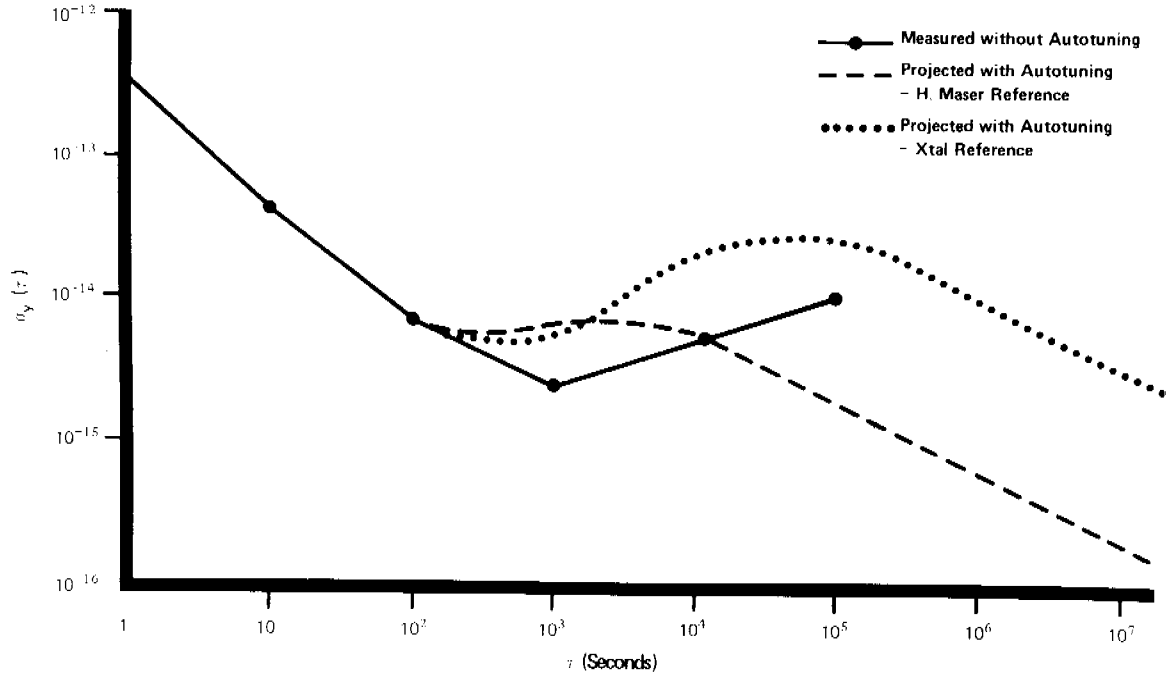

Figure 7. NASA Hydrogen Maser Stability

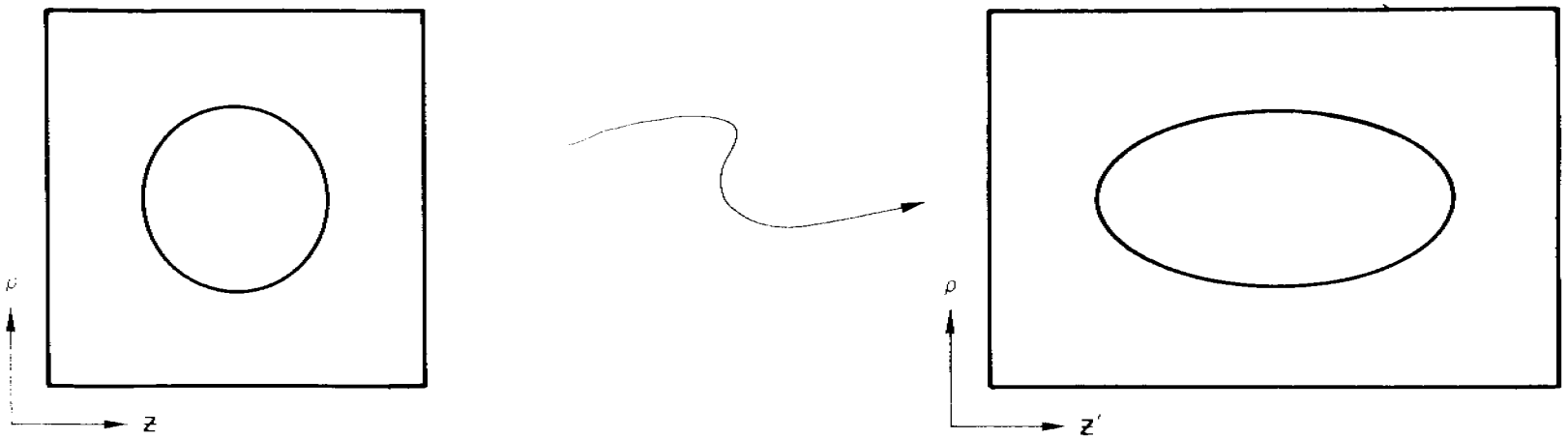

$$\eta'(G) = \frac{1.16806}{1 + \frac{0.16806}{G^2}} \eta'(G = 1)$$

Figure 8. Effect of Scale Change on η'

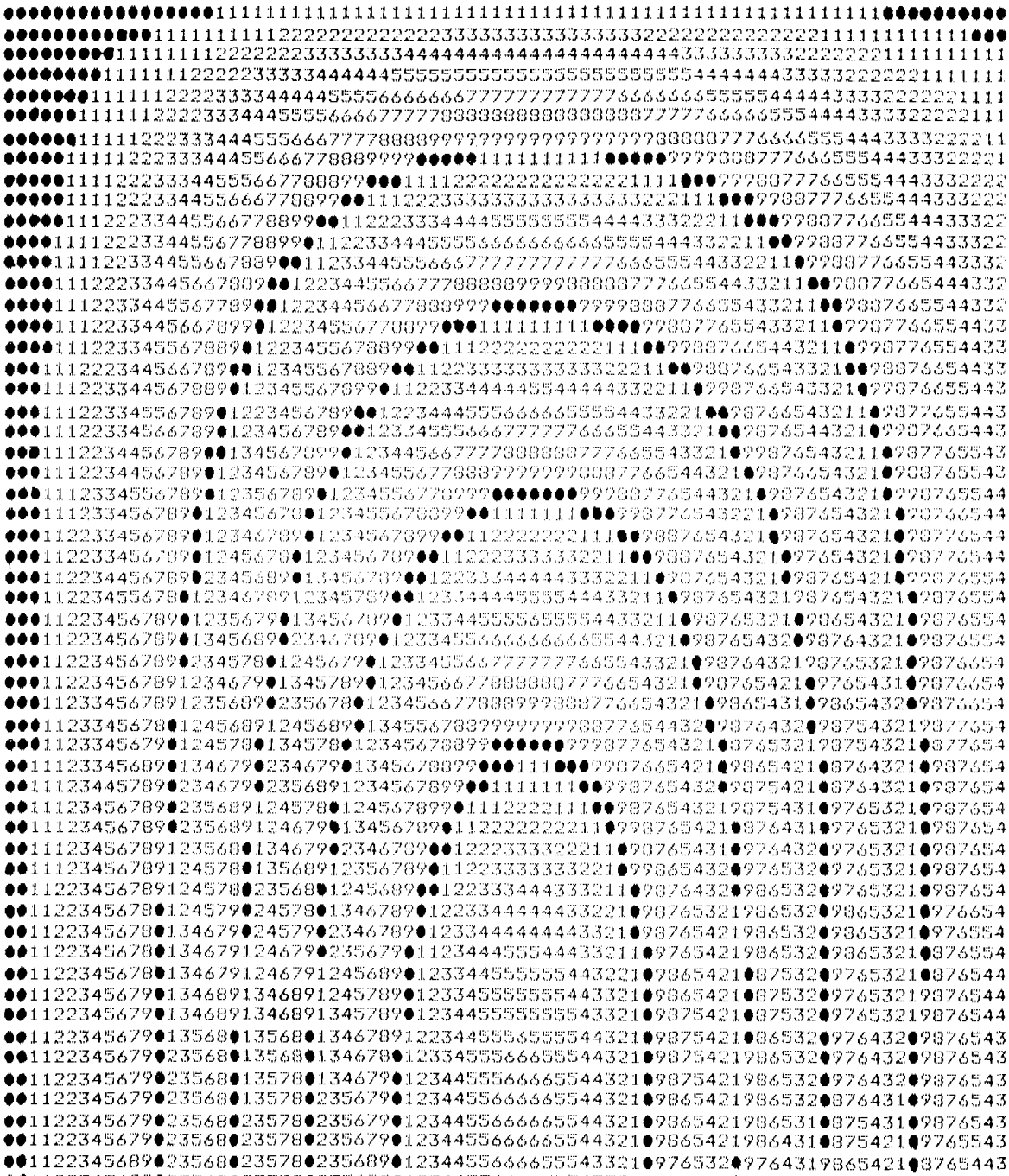

Figure 9. η' for Ellipsoidal Bulbs With g = 2